Asteroseismology of a Massive Pre-White Dwarf - Structural and Evolutionary Impact of Neutrino Cooling

Fernando Fonseca Vieira de Lima

January 23, 2021

Abstract

Neutrino emission is the most dominant process in what concerns energy loss for pre-white dwarf stars, and while there is consensus on the physics that is behind this cooling effect, the small interaction cross section of these particles makes it hard to experimentally test and corroborate the implications of this phenomena on a terrestrial laboratory. We make use of state of the art numerical code to model stars beginning in the ZAMS with masses ranging from $9M_{\odot}$ to $11M_{\odot}$ and evolving up to the white dwarf cooling sequence, and obtain their correspondent asteroseismic spectrum. Taking particular attention to the luminosity range of $L/L_{\odot} = 4$ to $L/L_{\odot} = 2$, where neutrino emission is the dominant energy loss mechanism, we study the impact of different non nuclear neutrino emission rates on the period spectrum of the g-modes, as well as the consequences of this impact on the star at a chemical and structural level. We identify a novel phenomena where a shift in the pattern of the period separation of higher order radial modes seems to take place when the neutrino emission rates are altered, whereas the pattern relative to lower order radial modes remains unchanged.

1 Introduction

White dwarfs are very dense stellar core remnants, presumably the final evolutionary stage of more than 97% of all stars. Resulting from low- and intermediate-mass hydrogen burning stars, these objects have reached a phase of their evolutionary process in which nuclear burning has ceased to be a significant energy source. Since no other energy source of the star is relevant enough to compensate for the continuously radiated (stored) thermal energy, it will begin to cool, becoming dimmer with passing time.

From a spectroscopic point of view, these objects can be classified as DA and non-DA white dwarfs, depending on the main constituent of their outer layers. DA white dwarfs represent the most abundant class, containing $\approx 85\%$ of all white dwarf stars ([15]), and it corresponds to such stars with hydrogen rich atmospheres, while non-DA white dwarfs correspond to these stars with hydrogen deficient atmospheres. This last class may be further subdivided according to their spectra and effective temperature, with DO white dwarfs presenting strong lines of HeII and with $45000K \leq T_{eff} \leq 200000K$, DB white dwarfs presenting strong HeI lines and with $11000K \leq T_{eff} \leq 30000K$ and DC, DQ and DZ presenting traces of carbon and metal in their spectra, and with $T_{eff} < 11000K$.

1.1 Neutrino Physics

The cooling of white dwarfs along their evolution is one of the main subjects of study in what concerns these stars, and any HR diagram containing the evolution of one of these objects indeed shows a characteristic evolutionary branch known as the cooling curve. Several analytical descriptions of this evolutionary branch are presently available or currently on the works, with the first and simplest being the Mestel model ([32]), which indeed captures the essential features of this cooling sequence, but it is derived with few and simple assumptions that do not include the many processes are known to occur along this path ([10,16,22]). One such process that has a significant impact at certain stages of this branch is the emission of neutrinos.

Neutrino production inside stellar interiors is a known phenomena that may occur due to several different processes ([3,33]) and results in the emission of these particles, which may represent a relevant energy sink in what concerns the energy balance of stars. Such is the case with white dwarfs, whose typical radii are far shorter than the mean free path of neutrinos, making it so that this could represent a source of energy loss during evolution. In a typical white dwarf, when nuclear burning ceases, the timescales of the surface luminosity drop and the central temperature drop differ, with the latter occurring over a longer period, which is a consequence of the large ratio between neutrino emission and the aforementioned surface luminosity ([11]), with this being the case during a significant amount of time during the evolution along the cooling curve, extending up to timescales of around $t \approx 10^7$ years ([2]). Since this neutrino dominated phase corresponds to the beginning of the cooling process, it is common to refer to these stars as pre-white dwarfs, noting that the spectroscopic classification of these objects is valid anyways. A very interesting class of variable stars that fall into this category are the well-known GW Vir stars, which are essentially variable DO white dwarfs (also known as DOV's) whose pulsations are gravity driven with typically low amplitudes. As already mentioned, stars at this stage have a characteristic chemical composition, lacking the typical hydrogen envelope that most white dwarfs have, and present higher temperature and luminosity than most white dwarfs, such that in this sense, they might effectively be considered pre-white dwarfs.

Among the many processes that are responsible for the production and subsequent release of non nuclear neutrinos inside of a white dwarf during this GW Vir stage, plasma-neutrinos represent the main energy sink, with the possibility of a considerable contribution of neutrino bremsstrahlung at later stages of the branch ([29]), noting that this last process implies a significant impact in the cooling of massive white

dwarfs ([20]).

It is interesting to reflect on the fact that, while there's consensus in what concerns the prevalence of neutrino cooling during this stage of evolution of white dwarf stars, it is a difficult task to replicate and experimentally test this phenomena in the laboratory, mainly due to the small interaction cross section of these particles ([19]), which in turn, makes it hard to verify certain predictions regarding their impact on the overall behaviour of this cooling stage, whether it be at a structural or at a phenomenological level. On the other hand, asteroseismology has been a consistent tool in what concerns the study of an array of topics regarding stellar structure and evolution, and naturally encapsulates the main aspects to consider when trying to approach the subject of the impact of neutrino cooling, effectively working as a metaphorical laboratory that allows for the verification of this neutrino print.

1.2 Massive White Dwarfs

An important consideration to take into account when studying white dwarfs is their mass distribution. These objects result from stars with masses up to $\approx 12M_{\odot}$ ([13]), with resulting masses theoretically reaching up to the Chandrasekhar mass limit ([5,6]), with a value of $1.45M_{\odot}$ for a C/O core white dwarf. Recently, white dwarfs with masses reaching up to $1.33M_{\odot}$ have been catalogued through the data acquired by the SDSS ([26]), and candidates with even higher masses ([17,21]), closing in on the limit were also identified after the Gaia Data Release (DR2) ([37]).

Recent studies resulting in mass distributions of select sets of white dwarfs ([28,31]) all seem to agree on a main peak of stars centered at around $\approx 0.6M_{\odot}$, with existence of a secondary peak at higher mass values of around $\approx 0.8M_{\odot}$ ([27]), and further analyzing isolated massive white dwarfs above this mass value reveals that a peak at $\approx 1.04M_{\odot}$ ([34]) is present. There seems to be indeed a significant number of massive white dwarfs with masses $> 0.8M_{\odot}$, presenting fractions of around $\approx 8\%$ of all catalogued white dwarfs, either it be DA or DB ([26]).

It is clear to see that massive white dwarfs represent a considerable fraction of the total population of these kind of stars. Not only this, but several particularities characteristic of said massive objects make them interesting subjects of study. For instance, massive white dwarfs represent the only type of these objects where Debye cooling is present at observable luminosities, since crystallization of the core occurs at also high luminosities due to their higher densities ([2,10]), hence making it so that these objects cool faster than their less massive counterparts as the luminosities decrease. Another feature of these objects is the fact that the temperature of their progenitors is presumably high enough to achieve stable carbon burning, making it so that O/Ne cores are possible ([16]), which is a relevant point to consider when studying the cooling of these massive stars, since the diffusion of this ^{22}Ne in the core may be responsible for the release of a non-negligible amount of gravitational potential energy that may impact the cooling time of these objects ([12]).

On the context of the cooling of these objects and on the topic of this article, it is important to mention the effect of neutrinos, which indeed influence the cooling times of white dwarfs, usually through the plasma-neutrino process ([18]), but in the case of these massive stars, neutrino bremsstrahlung must also be taken into consideration ([2,20]).This attribute, along with several other important factors, make massive white dwarfs great subjects of study in what concerns the influence of neutrino emission along their evolution. In particular, mass-radius relations for massive white dwarfs seem to show a notable dependence on the neutrino luminosity ([1]), and even beyond that, these stars seem to be the ones which exhibit a the most sensible temperature decay response to the neutrino luminosity in all the mass range of these kind of stars ([23]).

1.3 Precision Asteroseismology

As mentioned prior, GW Vir stars present multiperiodic, low-amplitude g-mode pulsations, and hence, we will be focusing on the study of g-mode spectra of modelled pre-white dwarfs. These modes can be theoretically computed by solving the fourth-order set of equations concerning linear, nonradial and adiabatic pulsations given in ([43]). It is easier to infer certain properties from these solutions making use of approximations such as the consideration of high radial order modes and also the Cowling approximation ([8]), which make it so that these modes respect the following dispersion relation:

$$k_r^2 = \frac{1}{\sigma^2 c_s^2}\left(\sigma^2 - L_l^2\right)\left(\sigma^2 - N^2\right) \tag{1}$$

This relation contains two relevant quantities in what concerns the analysis of the pulsation modes of the star, the first being the Brunt-Väisälä frequency:

$$N^2 = g\left(\frac{1}{\Gamma_1}\frac{d}{dr}ln(p) - \frac{d}{dr}ln(\rho)\right) \tag{2}$$

Which governs the g-mode period spectrum (low frequency modes), as can be seen by the direct dependence on the local gravity acceleration g. Additionally, $\Gamma_1 = \{\frac{dln(p)}{dln(\rho)}\}_{ad}$ is an adiabatic exponent and $c_s^2 = \Gamma_1 p/\rho$ is the square of the local adiabatic sound speed.

The second quantity is the Lamb frequency:

$$L_l^2 = l(l+1)\frac{c_s^2}{r^2} \tag{3}$$

Which defines the critical frequencies for p-modes (high frequency modes). These modes can be physically interpreted as radial displacements of the stellar fluid.

The relation defined by equation 1 allows for the mapping of the interior of the star in what concerns the propagation of modes, which is easily understandable when noting that pulsations only exist when the wavenumber is real. Considering the frequency σ of a certain mode, this can be achieved if $\sigma^2 > N^2, L_l^2$ which defines the resonant cavity where p-modes propagate, known as the p-region, or if $\sigma^2 < N^2, L_l^2$ which in turn defines the g-region.

When dealing with a g-mode spectrum, it is usual to study the evolution of the period of the pulsation modes, since these correspond to lower frequency modes which present periods whose timescales may correspond to values that are sensible enough so that they are prone to being measured. One of the main characteristics of the period spectrum of chemically homogeneous stellar structures is that in the asymptotic limit ($k >> l$), every consecutive radial order modes (k) with the same harmonic degree (l) have the same period spacing $\Delta\Pi_l^a$ ([41]):

$$\Delta\Pi_l^a = \Pi_{k+1l} - \Pi_{kl} = \frac{2\pi^2}{\sqrt{l(l+1)}} \left[\int_0^{R*} \frac{N(r)}{r} dr \right]^{-1} = constant \tag{4}$$

This is particularly interesting when considering the fact that typical models for GW Vir stars (and white dwarfs in general) present steep composition gradients which result in deviations from the behaviour established by equation 4. From a pictorial point of view, chemical interfaces work as reflecting boundaries inside of the star, making it so that if the length between boundaries matches the wavelength of a certain mode, it is possible to trap this mode as a standing wave, forcing it to oscillate with higher amplitudes in this trapping region. Trapped modes have their nodes confined to a smaller region, effectively making their periods seem shorter, and disabling the validity of a constant period separation value. The manifestation of mode trapping is then extremely dependent on the depth of the chemical transition regions inside of the star, as can be seen by the following analytical approximation, taken from ([24]), which expresses the periods of trapped modes:

$$\Pi_i^2 = 4\pi^2 \lambda_i^2 \left[\left(1 - \frac{r_c}{R}\right) l(l+1) \frac{GM}{R^3} \right]^{-1} \tag{5}$$

This expression refers to the trapped mode that contains i nodes between the surface and the chemical transition radius r_c, with λ_i being constants related with the roots of Bessel functions.

An important flag in what concerns mode trapping is the behavior of the oscillation kinetic energy of modes, which can be written as the following ([9]):

$$E_k = \frac{1}{2} GM^* R^{*^2} \omega_k^2 \int_0^1 x^2 \rho \left[x^2 y_1^2 + x^2 \frac{l(l+1)}{(C_1 \omega_k^2)^2} y_2^2 \right] dx \tag{6}$$

In this expression, y_1, y_2, y_3 and y_4 are the dimensionless Dziembowski variables ([14]), which are essentially eigenvalues, defined in order to solve the previously mentioned fourth-order set of equations that determine the pulsations. A^*, V_g and U are also dimensionless coefficients defined in order to further simplify the pulsation equations.

It's clear to see that, aside from the factors, this kinetic energy is proportional to the integral of some of the squared eigenfunctions defined as the Dziembowski variables, weighted by the density along the star. This then leads to the inference that modes propagating in deeper regions of the star, where the density is high, will have larger kinetic energy values, even when they are induced by small perturbations, while in turn, modes that are trapped in the outer layers of the star due to the steep He transition in the envelope will necessarily have small kinetic energy values. This makes it so that, similarly to the period spacing diagram, plots of the kinetic energy as a function o Π_k function as good indicators of trapped modes, since local minima of this function seems to indicate that a mode has less kinetic energy than it otherwise would have, were it not trapped,

Another interesting object that's worth looking into and may complement this period spectrum analysis is the weight function W_k of a mode with radial order k. Each mode runs through the star, presenting different amplitude values depending on the stellar structure and on how effective is the excitation mechanism. The relative values of weight functions serve as indicators on how the eigenvalues are settled along the star ([25]), and they may provide information regarding which regions of the stellar interior most contribute to the determination of the modes' periods. We follow the expression defined in ([9]), given by:

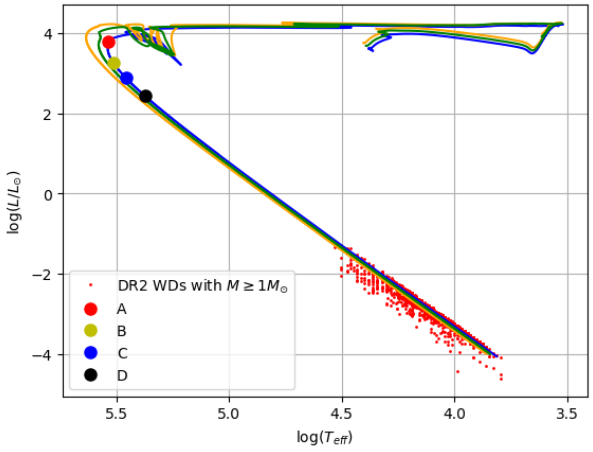

Figure 1: HR diagram containing the curves relative to the evolution of $9M_\odot$ (blue), $9.5M_\odot$ (green) and $10M_\odot$ (orange) initial mass stars from the ZAMS up to the white dwarf cooling sequence. Points A, B, C and D are benchmark evolutionary stages from the $9M_\odot$ initial mass star, chosen to study this region of evolution. Additionally, massive white dwarf candidates from GAIA ([21]) are shown at the end of the cooling sequences.

$$W_k = (4\pi G R_*^2) \frac{r^2 \rho^2}{R_*^2 U^2} \times \times \left[A^* y_1^2 + V_g (y_2 - y_3)^2 - \frac{1}{U} (l(l+1) y3 + y4)^2 \right] \tag{7}$$

This expression, just like the kinetic energy, is also written as a function of the same dimensionless variables that were mentioned above.

2 Evolutionary Code and Input Physics

In order to study the signature of neutrino emission in massive white dwarfs, an appropriate model was used to replicate the evolution of said stars. This was done using the MESA code ([36]), version r10398, with evolutionary input closely following the description present in ([30]), which details the evolution of both H and He atmosphere massive white dwarfs, starting from the ZAMS and reaching up to the oldest stages of cooling, where luminosity values are as low as $L/L_\odot \approx 4$.

Our models consist on different evolutionary tracks, concerning stars beginning at the ZAMS with masses ranging from $9M_\odot$ to $11M_\odot$, resulting in white dwarfs with $1.02M_\odot$ to $1.22M_\odot$, chosen with the intent of covering a wide range in which typical massive white dwarfs are present. Regarding the timezone in which we will focus our study, this being the initial track of the white dwarf cooling sequence, corresponding to an age range of $\log t[yrs] \approx 7.435 - 7.440$, the main input considerations are, as described in ([30]), the formulation of chemical diffusion and gravitational settling from ([4]), the absence of convection due to numerical instabilities, which has no impact on the cooling times relative to when convection is left active, and particularly does not affect the study of stellar pulsations and neutrino emission at this stage

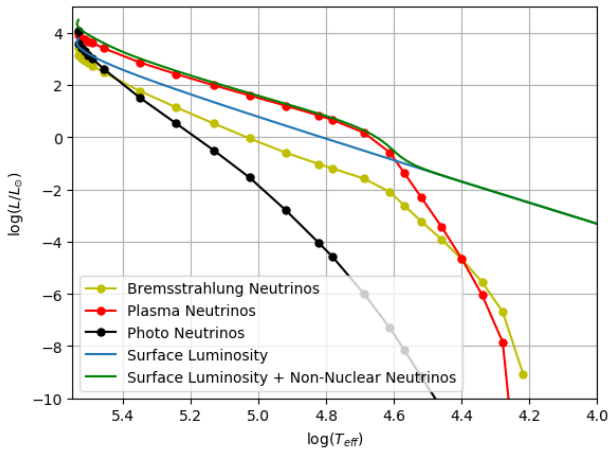

Figure 2: Weight of the several non-nuclear neutrino energy sinks for modelled $9M_{\odot}$ initial mass star, starting at the white dwarf cooling sequence.

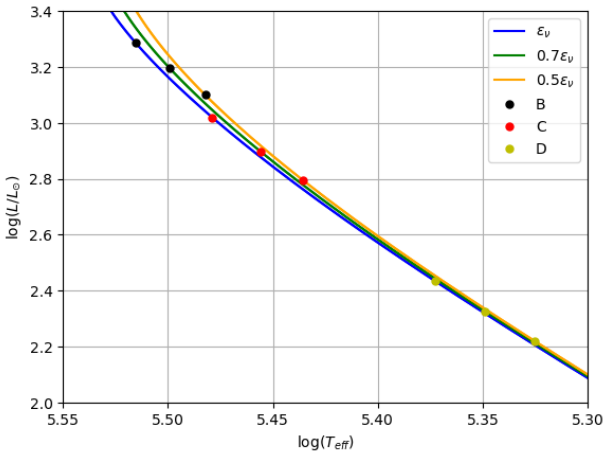

Figure 3: HR diagram containing the curves relative to the evolution of a $9M_{\odot}$ initial mass star, each with different initial neutrino emission rates, these being the unchanged rate of ϵ_{ν} (blue), $0.7\epsilon_{\nu}$ (green) and $0.5\epsilon_{\nu}$ (orange). Each curve contains their respective benchmark points A, B and C, where each set of points with the same color across all curves correspond to comparison evolutionary points.

of the evolution, since at this stage (GW Vir stage), convection is yet to set in and pulsations are mainly excited by the $\kappa-$mechanism ([38]). Lastly, the emission rates for plasmon, brehmsstralung and several less important neutrino sources are taken from ([20]).

Resulting HR diagrams from our models are shown in figure 1, as well as the benchmark profiles chosen for one of the models, to probe the region where neutrinos represent the largest energy sink. The selection of these profiles is based on the information conveyed in figure 2, which allows to compare the impact of several different energy sinks with the surface luminosity of the star as a function of T_{eff}.

Regarding the seismology component of this work, the pulsation eigenmodes of our models were obtained making use of the GYRE oscillation code ([42]), version 5.1, using the MESA models as direct input and using the formulation of ([7]) in what concerns the boundary condition of the shooting method used in the search. An inverse frequency grid type (uniform in period) is also used in order to more easily scan for adiabatic g-modes.

3 Neutrino Emission Rates

The main purpose of this work is to study the impact that neutrino cooling has on the overall evolution of pre-white dwarf objects while neutrinos are still the most relevant energy sink. For this reason, and due to the numerical nature of the models, a similar prescription to that of[35] was used, in which the emission rates of non nuclear neutrinos was manually altered before the star enters the white dwarf cooling sequence. This then allows to compare models relative to the same star but with different neutrino emission rates and detect any changes which, as a result, will necessarily be a direct or indirect consequence of the neutrino effects on the cooling of the star.

Starting from the benchmark points shown in figure 1, we reproduce the same model, which in this case corresponds to the $9M_{\odot}$ initial mass model, up to the first of these points, this being profile A, and at this point, we alter the neutrino emission rate by a certain factor, making it so that the evolutionary track is slightly changed from this point on. Figure 3 shows how the evolutionary track is altered by considering situations where at point A, the neutrino emission rates are set to 50% and 70% of the original rate, these being represented in orange and green respectively, relative to the model with unaltered rates, represented in blue. As for the comparison points, which are also represented in the figure, where each set of points with the same color represent comparison points, these were selected such that the current neutrino rate of the unaltered model multiplied by the factor of the altered model, is equal to the current neutrino rate of the altered model, i.e., the neutrino emission rates of point B relative to the orange curve is, at that point, half of the neutrino emission rate of point B relative to the blue curve.

Furthermore, figure 4 shows how the main unaltered sources of neutrino emission change as the star evolves, both in terms of position in the star and intensity. As mentioned prior, plasma neutrinos are the dominant energy source during this pre-WD phase, and along with the energy due to bremsstrahlung neutrinos, which are also relevant when considering such high mass values, both make up for almost the totality of energy lost during this phase. From this figure, we notice how the production of these neutrinos moves outwards along the star as they decrease with time, and for this reason we don't extend the analysis to much later times relative to profile C, because it's clear to see that the neutrino emission rate dies off if we move ahead in time.

4 Precision Asteroseismology and Analysis

We now proceed with the analysis of the impact of altered neutrino rates on the structure and evolution of the model. We begin by discussing some of the properties that are usually relevant in typical spectra of massive (and overall) white dwarf pulsation. To this end, we can start by analyzing the evolution of propagation diagrams along the region in study.

The first row of Figure 5 shows exactly how this takes place, containing, from left to right, the corresponding diagrams relative to the profiles A, B and C present in Figure 1, concerning a $9M_{\odot}$ initial mass star and evolving into a $1.02M_{\odot}$ white dwarf. In this figure, both the propagation diagrams and the chemical profiles contain information regarding the star as it would normally evolve, and the case where neutrino emission rates were set to half (orange curve in figure 3), with this being

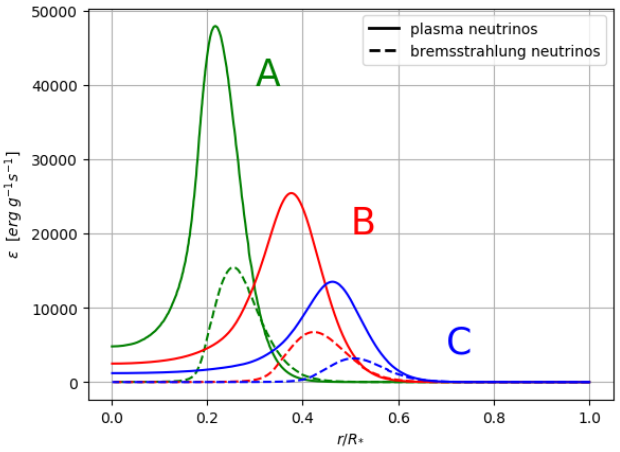

Figure 4: Neutrino emission rates relative to benchmark points A, B and C concerning the modelled $9M_{\odot}$ initial mass star with unchanged neutrino emission rates. Continuous lines refer to plasma neutrino emission rates while dashed lines refer to bremsstrahlung neutrino emission rates.

represented with dashed lines. The situation corresponding to the rate reducing factor of 0.7 is not represented in these diagrams in order to keep the figure visually clear, but the shape of the lines concerning this case is evident, as this represents a midway point between the two cases that are shown.

Profile A, which is the common point between the cases, depicts the star right before T_{eff} achieves its maximum value, being at $T_{eff} = 341491K$ and with $\log(L/L_{\odot}) = 3.79$, and for this reason, it presents some similarities with typical red giants diagrams, which correspond to a previous stage of evolution in the lifetime of this star. In this regard, it can be seen that the central values of N^2 are comparable to the outer values, and some dips in this frequency structure allow for the presence of some mixed modes. This trait vanishes as the star keeps evolving through this neutrino phase, with N^2 increasing in value in the outer regions of the star, making it so that there is a wider gap between the G- and P-regions and no mixed modes seem to be possible. The propagation diagrams relative to profiles B and C clearly illustrate this point, with the correspondent chemical profiles revealing that this is accompanied with a settling of several layers in the star, with the outer carbon layer being the most evident. It is then interesting to compare the situation between the case where neutrinos are unaltered and the case where their rate is set to half. As seen in the figure, there's a clear agreement between the abundance curves at the inner regions of the star, but the outer layers seem to have a small departure from one another as the evolution goes on, as can be seen by the helium and carbon curves, indicating that the effects of gravitational settling are stronger when neutrino emission is halved, which is in agreement with the fact that the model with halved neutrino takes approximately double the time to reach point B when compared with the model where rates are unchanged.

As mentioned prior, GW Vir stars are known to pulsate with low amplitude g-modes, and for that reason, the focus of the seismologic analysis in this work is done according to the eigenmodes present in the G-region of the evolving propagation diagram of the star. We instill particular attention to the blue dashed line present in the propagation diagrams of B and C, which corresponds to the frequency of the mode g_{60} (radial order $n = 60$ and angular degree $l = 1$), which we choose as a reference mode due to the fact that it is one of the lowest radial order g-modes that is allowed to propagate up to the surface during most of the time range on which our study is focused on, and theoretically, would be one of the easiest to detect.

5 Neutrino Sensitivity Function

To further the study of this mode, we make use of the expression given in equation 7 to obtain the correspondent weight function, which is depicted in figure 6 at several stages of evolution of the star. Additionally, the first row in this figure represents the case where the neutrino emission rates are unchanged, with the letters A, B and C referring to the profiles to which these weight function applies. The second row refers to the case where the emission rate was set to half, and each lower panel corresponds to a profile of the altered star where the neutrino luminosity is half of the luminosity of the profile in the correspondent upper panel. The lines present in each panel correspond to the plasma (orange) and bremsstrahlung (green) neutrino emission rates associated to that profile, with all cases being normalized to the maximum value of the first panel of the correspondent row.

One interesting characteristic of the weight function, regardless of the row that is being considered, is that its maximum value seems move from close to the core up to the surface as time goes by, which seems to be the case when considering lower mass white dwarfs, as seen in other works ([9,25]), meaning that the zone most contributing to the generation of this mode transitions outwards as the star cools. It is worth mentioning that all modes with $k > 10$ present a very similar behavior to this one, the only difference being the number of nodes, which evidently correspond to k itself, which means that the aforementioned statement regarding the region where the mode is most prevalent, as well as further analysis concerning this g_{60} mode also applies these lower order modes. This particular outward shifting effect that we just assessed is a consequence of a decrease in central condensation in the star, as described in ([39]).

Perhaps the most interesting feature of this figure, which coincidentally also refers to an outward displacement, granted that this time we're referring to the well defined peak seen in each panel and not the overall maximum value, is how the normalized neutrino curve seems to resemble this prevalent peak in the weight function, both in shape and position, as they move outwards and decrease along this cooling period. Both these peaks seem to follow the small region just outside the C/O core where there's a drop in oxygen and carbon, and an increase in neon, which corresponds to the region where off-center carbon ignition occurred ([40]), and hence represents the hottest region of the star during this neutrino dominated period. This attribute more or less explains why the neutrino emission rates are prevalent in this area, since it is the region that most easily excites the pair production from plasmons, but no evident connection between this neutrino production area and the peak in the weight function can be deducted.

In order to more or less quantify this apparent relation between these two quantities, we define a neutrino sensitivity function S_{ν_k}:

$$S_{\nu_k} = \frac{\int_0^r 4\pi r'^2 \rho(r')\epsilon_\nu(r')W_k(r)dr'}{L_\nu} \tag{8}$$

This function is taken at a certain temporal point of the evolution, with ϵ_ν being the rate of non-nuclear neutrinos

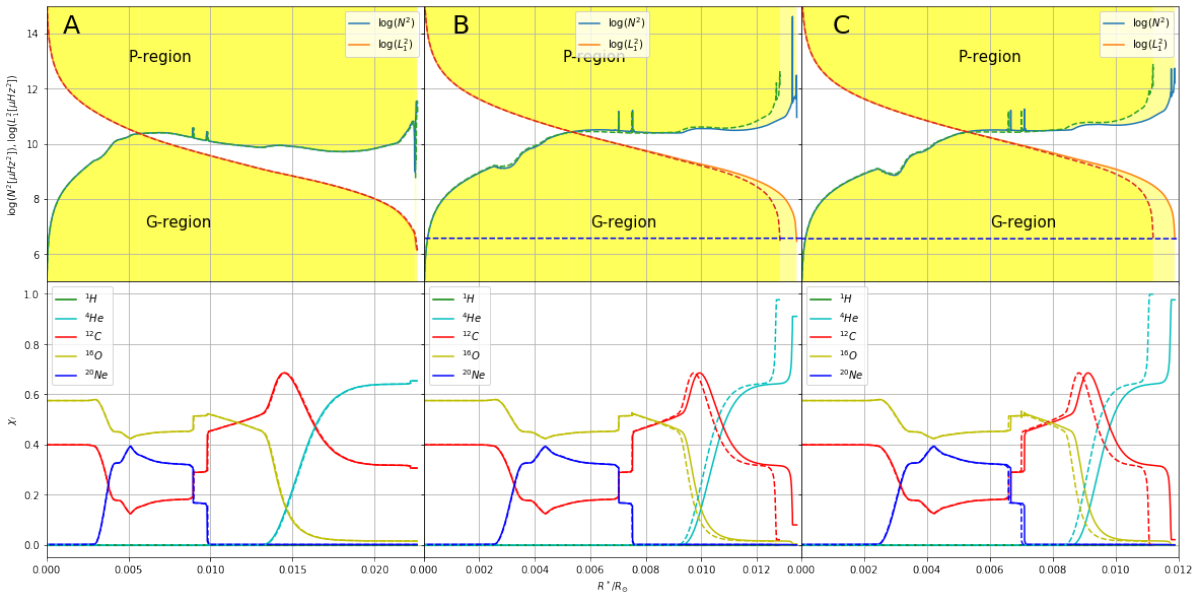

Figure 5: Propagation diagrams (first row) and chemical profiles (second row) of $9M_{\odot}$ initial mass star models. Continuous lines refer to the model where neutrino emission rates are unchanged and dashed lines refer to the case where neutrino emission rates are halved. A, B and C labels are representative of the benchmark points chosen for each model

along the star at this temporal point, W_k being the normalized weight function of the g_k mode also at this point, and $L_\nu = \int_0^{R*} 4\pi r^2 \rho(r)\epsilon_\nu(r)dr$ being the non-nuclear neutrino luminosity, which essentially corresponds to the integral in the numerator of equation 8 without the weight function, meaning that this sensitivity function will only present values between 0 and 1. This function is designed with the intent of verifying how sensible the g-modes are in what pertains to the decaying neutrino rates as the evolution proceeds, and hence why the numerator of this expression is chosen as a "weighted" version of the neutrino luminosity function, directly relating these two quantities across the entire stellar structure. Looking at the shape of both functions in each panel of figure 6, it is expected that this sensitivity assumes a similar behavior to that of a step function, with a very steep increase characterized by an inflexion point right where both peaks assume their maximum value, making it so that, as time progresses, this inflexion point moves outwards and the upper threshold decreases, assuming that the peak of the weight function ceases to be the overall highest value of this function as it happens in the first row of the figure.

It is of interest to analyze how the sensitivity function of different modes behave as the star evolves, and specially how it compares between the cases with different neutrino emission rates. Figure 7 contains several points concerning the maximum value (upper threshold) of the sensitivity function of different radial order g-modes at several stages of the neutrino cooling process as a function of the surface luminosity. Points connected by a continuous line represent modes concerning the model where neutrino rates are unaltered, while points connected by dashed lines represent modes concerning the model where rates were halved.

It is clear to see that in most cases, regardless of the fact that the rates of neutrino emission were changed or not, there is a common behavior in which the sensitivity seems to decrease with time, which agrees with the fact that the peak of the weight function decreases with time relative to the absolute maximum of this function. This behavior however seems to only be established when we consider modes with $k \geq 10$, since modes such as g_1 and g_5 seem to respond in a different manner, presenting increasing sensibilities at certain stages. This seems to agree with the previously mentioned fact that modes with lower radial orders, specifically $k < 10$, have weight functions with a considerably different shape than the others, partly due to having a lesser amount of nodes, but mostly due to how their envelopes are more evenly distributed along the star, not showing many evident peaks as is the case with the envelopes of weight functions of higher radial order modes. Nonetheless, the existence of fewer nodes in the weight functions of these lower radial order modes makes it so that, if any of the peaks of this function fully encapsulates the peak of the neutrino emission rate, then the integral present in S_{ν_k} will increase relative to the case where a similar valued oscillatory weight function takes the same position. This trait explains the increases that might be present in the evolution of the sensitivity function of lower radial order modes.

Another interesting subject regarding this figure is how the functions concerning the altered and non-altered neutrino emission rates compare to each other. This, once again, seems to have a certain dependence on the radial order of the modes that are being considered, and while the number of points available should be increased in order to study this feature in more detail, it is more or less apparent that higher radial order modes seem to be the ones that are more sensible to changes in the rates of neutrino emission. Indeed when comparing the values of this function relative to a single mode in the case where neutrino rates are unchanged to the values of the function relative to this same mode but with the rates halved, it is indisputable that they do not match for any mode, even taking into account the small sampling size that is being used. However, it is also clear that this mismatch is much more evident as the radial order of the mode that is being considered increases, with a noticeable gap between the continuous and the dashed line forming at around $k = 10$ and seemingly increasing as we consider higher k values. This gap forms as a consequence of the fact that the sensitivity values are higher along the evolution of the star when the rates halved, which is something that can be understood by looking at figure 6 and

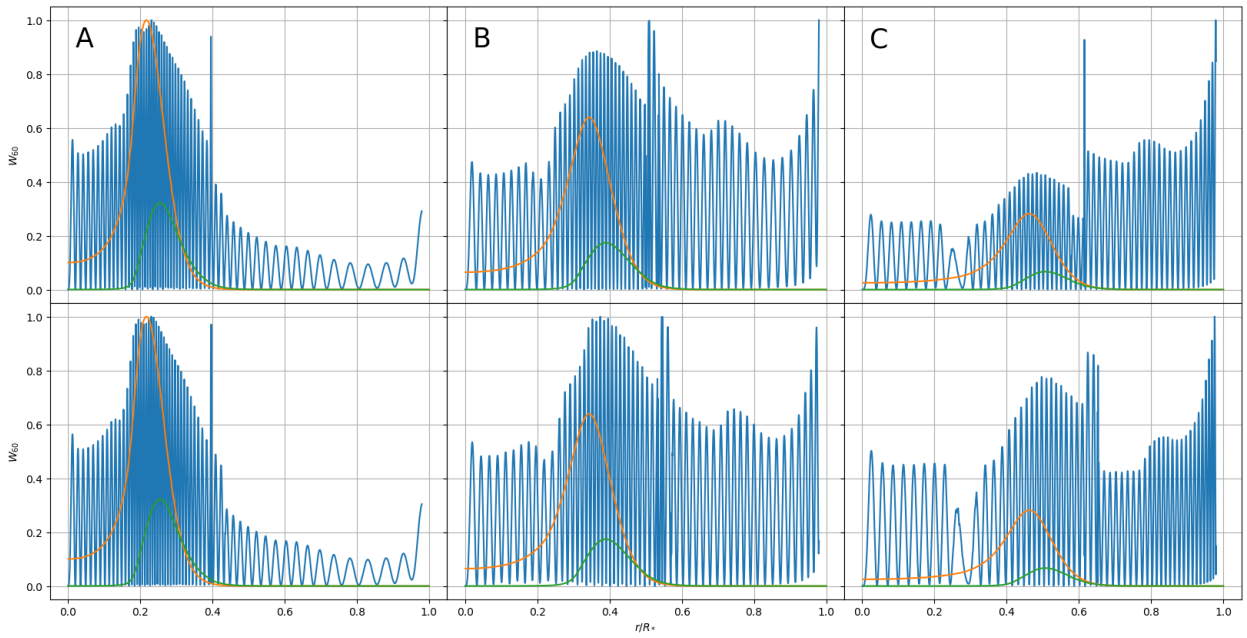

Figure 6: Weight functions of g_{60} mode at different evolutionary points of modelled $9M_\odot$ initial mass star with unchanged neutrino emission rates (first row) and halved neutrino emission rates (second row), as well as plasma (orange) and bremsstrahlung (green) neutrino emission rates normalized to highest value of correspondent row. Just as in figure 5, A, B and C labels are representative of the benchmark points chosen for the model with unchanged rates, while the correspondent comparison points for the model with halved rates are chosen such that at each column, the neutrino emission rate of the model of the lower panel is half of the rate correspondent to model with unchanged rates in the upper panel.

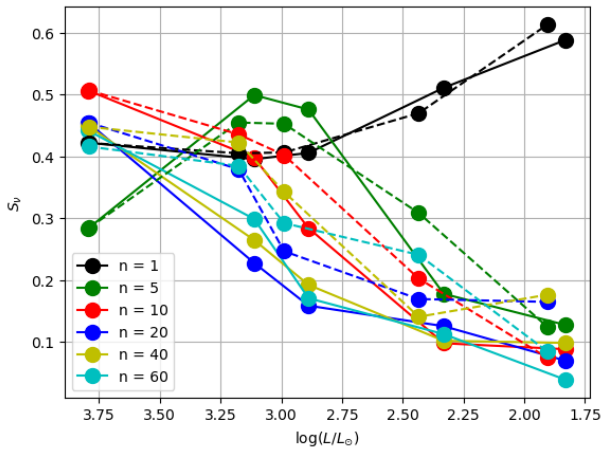

Figure 7: Evolution of the sensitivity function given in equation 8 for different radial order g-modes for modelled $9M_\odot$ initial mass star. Continuous lines refer to the model where neutrino emission rates are unchanged and dashed lines refer to the case where neutrino emission rates are halved.

noticing the differences between the weight functions present in the upper and lower panels of the last two columns. In the case where neutrino production is halved, this being the second row, the maximum values of the peak's envelope that is being considered are considerably higher after normalization than those of the first row. As a consequence of this fact, the area below the smaller width peaks that are encapsulated by the envelope and also encapsulated by the neutrino emission peak, or in other words, the integral of the product of these two functions, is higher, which is easily understandable when noticing that these peaks "close" slower as they grow into their maximum value due to having a higher value to grow into when compared to the case where the rates are unchanged. This effect becomes more and more drastic as we increase the radial order of the mode, which indicates that the amplitudes of the weight functions of these modes are the most affected by changes in the rates of neutrino emission as the star cools.

6 Neutrino Induced Trapping Phase Shift

The analysis performed making use of the sensitivity function suggests that the rate of neutrino emission at a certain point of evolution of a pre-white dwarf has a direct or indirect influence on the pulsation modes of the star. This inference regarding the sensitivity of pulsation modes was done through a graphical analysis of a function that suggests, but does not imply correlation. It is then instructive to further extend the exploration of the impact of neutrino emission to defining and measurable properties of pulsation modes. To this end, we will study the evolution of the period separation pattern during this phase, which is shown in figure 8, where each panel corresponds to one of the previously mentioned profiles in what concerns the model where neutrino emission rates are unchanged. In this figure, points connected by a continuous (blue) line once again refer to this model, whereas points connected by a dashed (black) line correspond to the model where rates were halved. Additionally, the dashed, horizontal line (red) corresponds to the period spacing asymptotic limit, given by equation 4, concerning the model with unchanged rates, noting that while the asymptotic value relative to the model with halved rates is not represented, it practically matches the previous case.

At first glance, it is evident that neither of the patterns correspond to the behavior established by the asymptotic limit, which is to be expected due to the fact that our models contain several composition gradients that, as mentioned previously, may work as reflecting boundaries for certain modes, which makes it so that various resonant cavities may be identified throughout the star, these being evident by looking at the chemical profiles of figure 5. The direct consequences of these

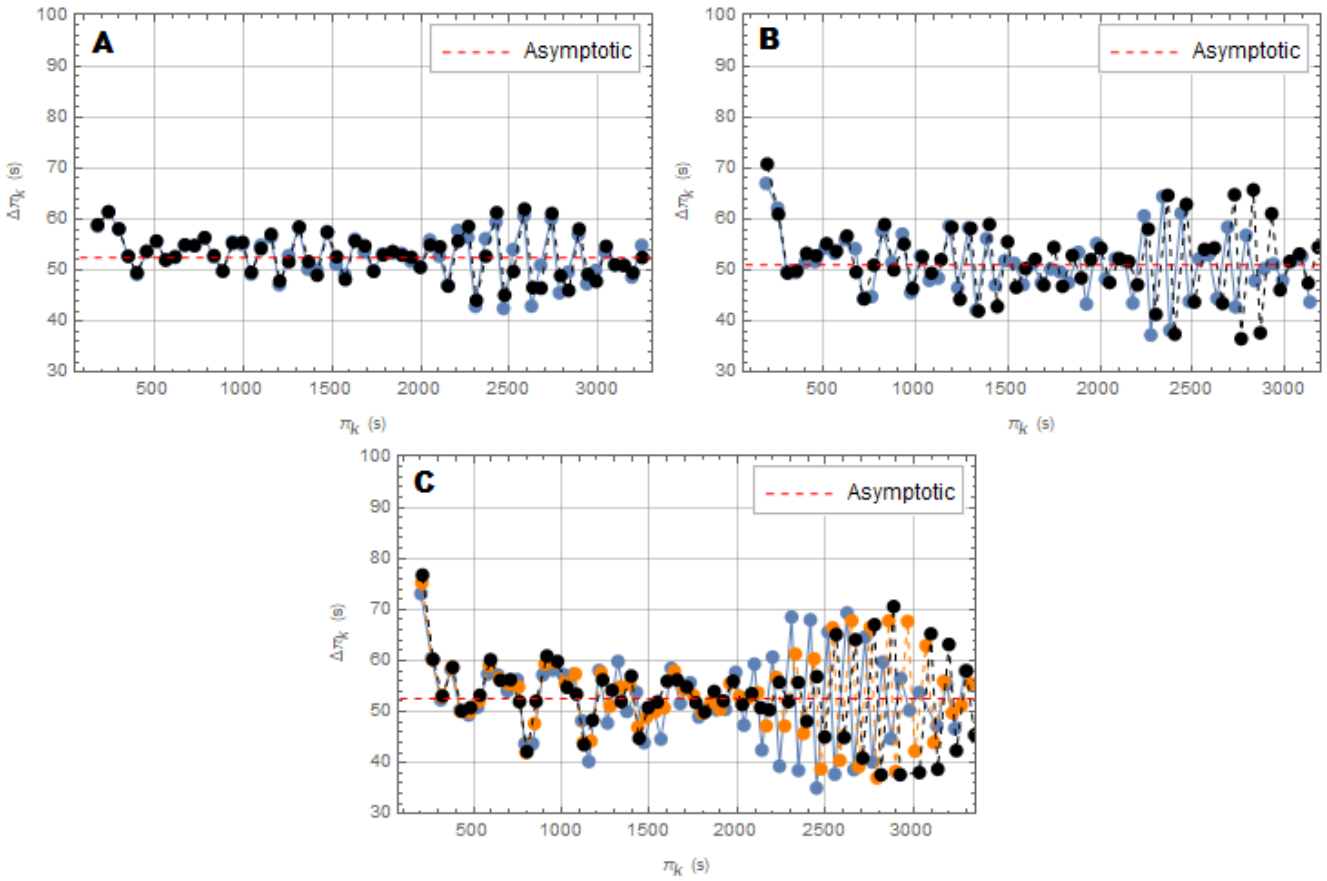

Figure 8: Evolution of the period separation $\Delta\Pi_l^a$ of the g-mode spectrum for modelled $9M_\odot$ initial mass star. Once again, continuous blue lines refer to the model where neutrino emission rates are unchanged, black dashed lines refer to the case where neutrino emission rates are halved, orange dashed lines refer to the case where neutrino emission rates were set to 70% and the A, B and C labels are representative of the benchmark points chosen for the models. The red, horizontal dashed line in each panel corresponds to the value of the period separation in the asymptotic limit given in equation 4 concerning the model with unchanged rates.

cavities is that modes with wavelengths identical to their sizes might get trapped inside, in return presenting changes in their periods, which may then be mirrored onto the values of the period separation, since the distance relative to the periods of adjacent modes in radial order (which coincidentally, might also have their own periods altered due to this same effect) is altered as well. This creates a situation where $\Delta\Pi_l^a$ for a certain k mode becomes higher or smaller in value, and deviates from the expected behavior, hence creating the maxima and minima that can be observed in the period separation patterns of our figure. This trapping occurrence is of particular interest in what concerns predicting what modes might be impossible to measure even though they are excited, since they may be enclosed in the resonant cavities inside of the star, this being done with a correct identification of the extrema in the pattern and the respective mode and cavity that is causing them.

That being said, there is an interesting feature that can be identified in this figure once a comparison between the patterns generated by our two models is done, and that is the progressive shift of the rightmost part of the pattern corresponding to the model with halved neutrino emission rates relative to the model with unchanged rates, as both evolve. As can be seen on the first panel, both patterns seem to match entirely, which is expected since profile A correspond to the point of evolution where the rates of the second model were set to half, effectively working as the initial point of the cooling phase in study, but as we look further in time, there seems to be a slight localized displacement of the dashed pattern to the right, relative to the continuous pattern. This displacement begins to be noticeable at stages close to the temporal point where profile B is located, where from figure 4, plasma-neutrino rates are of around $\epsilon_{\nu_p} \approx 25000\ erg \cdot g^{-1} \cdot s^{-1}$, and half of that value in the case of the second model, and it seems to be completely established at the evolutionary point represented by profile C, where the rates are now close to half than the ones in B, and neutrinos start to become less and less relevant moving forward. It is important to mention that this clear pattern that is being shifted contains several local minima and maxima of the period separation, which suggests that the modes relative to these points are being subject to trapping.

Another interesting trait from this result is that this displacement appears to occur only when considering higher period modes, starting at around $\Pi_k \approx 2000s$, which interestingly correspond to higher radial order modes, with $k \gtrapprox 30$, meaning that the direct or indirect effects of altering the neutrino rates of the star seem to have an impact on these modes while leaving lower order modes unaltered, which agrees with our previous assessment that higher radial order modes are more sensible to changes in the rates of neutrino emission.

This pattern shift seems to be a consequence of various factors in which neutrino emission seems to be a relevant factor, namely the propagation regions for g-modes inside the star, as well as the chemical profiles. Indeed when looking at figure 5, there is a clear displacement of the outer chemical transition interfaces between both models, which also seems to become more evident as time progresses. This feature makes us re-

Table 1: Values of equation 9 for the different transition regions defined in figure 9

$(\Pi_{50}/\Pi_{100})_{r_{c_1}}$	$(\Pi_{50}/\Pi_{100})_{r_{c_2}}$	$(\Pi_{50}/\Pi_{100})_{r_{c_3}}$
0.945	0.946	1.194

fer to equation 5, which shows the dependence between the periods of trapped modes and the radius of these transition regions r_c, with these being effectively different when looking at the outer layers of both models, but maintaining the same values when considering the inner regions. This in turn makes it so that the trapping effect occurring at the outer regions of the model with halved neutrino emission rates suffers a shift in what concerns the periods of the modes that are being subject to this effect, relative to the model where neutrino emission rates are unchanged, while the periods of modes that are trapped in the innermost regions of the star are unaltered. We may quantitatively assess this effect by using equation 5 to write an appropriate expression that allows for the comparison of the periods of trapped modes in the case where neutrino emission rates are unchanged, which we label as Π_{100} with the periods relative to the case where rates are halved, labelled as Π_{50}:

$$\left(\frac{\Pi_{50}}{\Pi_{100}}\right) = \sqrt{\frac{\left[\left(1-\frac{r_{c_{100}}}{R^{*}_{100}}\right)\frac{M^{*}_{100}}{R^{*3}_{100}}\right]}{\left[\left(1-\frac{r_{c_{50}}}{R^{*}_{50}}\right)\frac{M^{*}_{50}}{R^{*3}_{50}}\right]}} \tag{9}$$

This expression eliminates the original dependence on λ_i since it intends to compare the modes that are subject to trapping as a consequence of a chemical interface r_c and contain the same amount of nodes between this interface and the surface, even though the interface is shifted between models.

It is now necessary to define the values of r_c relative to the interfaces that might be the reason for the trapping. As mentioned previously, this effect is a consequence of steep chemical interfaces in the interior of the star, such as the inner transitions from the core to outer layer, or even the steep transition to the He envelope. A useful diagnostic of what chemical interfaces might be relevant in what concerns this effect is the Brunt-Väisälä frequency N^2, since its dependence on dp/dr and $d\rho/dr$ will reveal some spikes in this structure as a consequence of discontinuities in pressure and density, which are typical traits of chemical transition regions. With this in mind, and focusing on profile C, three different transition regions were selected for each model with their r_c being represented by the colored dashed lines in figure 9.

Additionally, table 1 contains the values given by equation 9 relative to the transition regions defined in figure 9. Each of these values corresponds to ratio between the periods of modes trapped in the correspondent transition layer in the model where neutrino emission rates are halved and the model where these rates are unchanged. This seems to indicate that the shift of the rightmost pattern must be caused by the outermost transition region due to the He envelope, since the value for this ratio seems to correspond to the same ratio between the periods in which this pattern is present for each model. As for what modes are the ones being affected, the propagation diagrams seem to show that the region of the star in which g-modes propagate grows with increasing radial order, with modes starting at approximately $k \gtrapprox 30$ in radial order reaching this layer, meaning that this predicted shift of

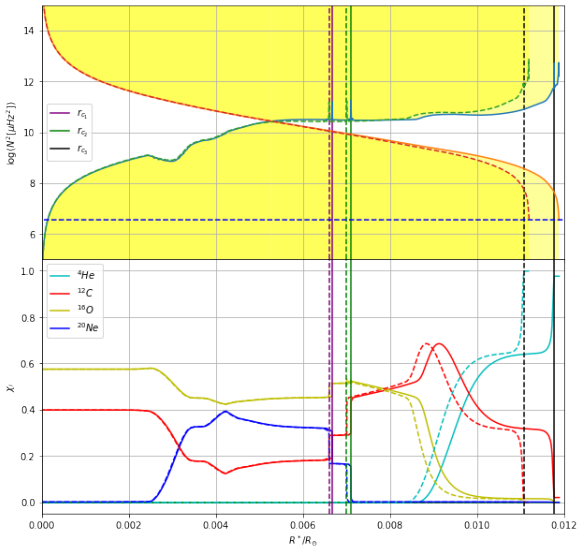

Figure 9: Propagation diagrams (first row) and chemical profiles (second row) relative to profile C of $9M_\odot$ initial mass star models. Continuous lines refer to the model where neutrino emission rates are unchanged and dashed lines refer to the case where neutrino emission rates are halved. A, B and C labels are representative of the benchmark points chosen for each model. The coloured vertical dashed lines correspond to the r_c of the steep chemical interfaces that might be responsible for mode trapping, and are identified according to the label in figure

trapped modes' periods should only be noticeable for higher radial order modes, which agrees with the results shown in figure 8.

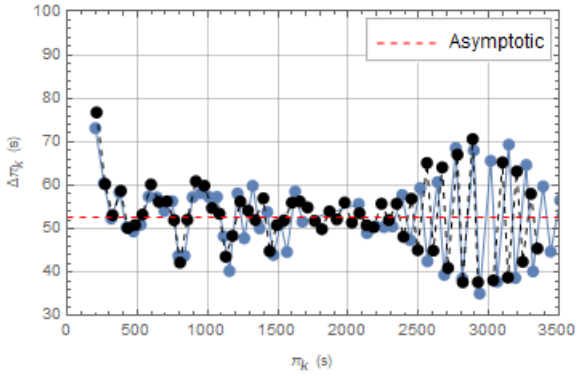

Figure 10: Evolution of the period separation $\Delta\Pi_l^a$ of the g-mode spectrum for modelled $9M_\odot$ initial mass star, with periods of trapping pattern relative to the model with unchanged rates corrected by the appropriate factor given by equation 9 for the He transition region. Continuous blue lines refer to the model where neutrino emission rates are unchanged and black dashed lines refer to the case where neutrino emission rates are halved.

If we indeed shift the the periods of the model with unchanged neutrino rates in which this pattern seems to occur (starting at $\Pi_{30} \approx 1700s$) by the equation 9 factor correspondent to this layer, we see that the patterns of both models almost coincide as can be seen in figure 10, which is a strong evidence to support the claims that indeed this trapping is being caused by the outer He layer, and that this trapping effect is dependent on neutrino emission rates of the star, which indirectly alter the periods of the modes that are being subject to this effect.

7 Conclusions

We started by studying the direct impact of altering neutrino emission rates on a model corresponding to the same star, choosing points of equal percentage of neutrino energy loss as comparison points across all models, with this revealing that an amount of time proportional to the neutrino reducing factor of each model is needed in order for these points to be reached, this being accompanied with slight differences in the major global quantities of each model, but overall consistency in regards to the previous evolutionary track at each point. The model used for analysis along the work was one corresponding to a $9M_{\odot}$ initial mass star, but the conclusion presented ahead are verified when considering higher mass models, up to $10M_{\odot}$. The main inference that can be extracted from the comparison of the models at each point is that the neutrino emission rate directly and indirectly affects the behavior of the evolution along this track, as can be detected by simply looking at the distinct tracks of the HR diagram that are created as a consequence of models with distinct neutrino emission rates, but also by analyzing the chemical stratification of each of these models, which are subject, during longer or shorter periods of time, to all the additional phenomena respective to this evolutionary stage, namely the onset of gravitational settling, depending on the duration between comparison points, which is exclusively dictated by the rates of neutrino emission. Differences concerning the evolution of the period spectrum of each model are obviously present locally in time as a consequence of the different stages of prevalence of each evolutionary phenomena in effect, which enhances the necessity of different temporal comparison points, but the overall progression of each mode of the spectrum seems to agree between models.

In the second part of this work, the focus of the study concerning the impact of neutrino emission was shifted to to the propagation of modes in the interior of the star. To this end, we made use of the weight functions of each mode and locally compared them to the respective neutrino emission rate curve, noticing a similarity in their behavior as the star cools. While this effect occurs independently of the rates, some differences concerning the inner amplitudes of the weight functions are present, where it seems that in each comparison point, the higher the neutrino emission rates are, the smaller are the inner values of the weight function. To quantify this effect, we defined a neutrino sensitivity function, whose progression along the evolution of the star may be compared between models and allowed to infer that the weight functions of the modes (and hence the modes themselves) that are most affected by changing neutrino emission rates correspond to those of modes with higher radial orders.

In order to obtain the impact of neutrinos on measurable properties of the pulsation modes, we last compared the period separation and kinetic energy of our distinct neutrino rates models, and verified the onset of a displacement of the pattern of the period separation relative to higher radial order modes, with $k \gtrapprox 30$. We verified that this pattern was being caused due to trapping of these modes, and concluded that the pattern shift was a consequence of the displacement of the He envelope transition layer between models with different rates, effectively presenting a method of deducing that this layer is responsible for the trapping of high order radial modes during this evolutionary stage, and most importantly establishing, as a complement of the analysis of the sensitivity function, that changing neutrino emission rates impact the propagation and overall behavior of these same modes.

References

[1] Althaus L. G., García-Berro E., Isern J., Córsico A. H., 2005, Astronomy & Astrophysics, 441, 689–694
[2] Althaus L. G., Córsico A. H., Isern J., García-Berro E., 2010, The Astronomy and Astrophysics Review, 18, 471–566
[3] Barkat Z., 1975, araa, 13, 45
[4] Burgers J. M., 1969, Flow Equations for Composite Gases
[5] Chandrasekhar S., 1935, Monthly Notices of the Royal Astronomical Society, 95, 207
[6] Chandrasekhar S., Milne E. A., 1931, Monthly Notices of the Royal Astronomical Society, 91, 456
[7] Christensen-Dalsgaard J., 2008, Astrophysics and Space Science, 316, 113–120
[8] Cowling T. G., 1941, Monthly Notices of the Royal Astronomical Society, 101, 367
[9] Córsico A. H., Althaus L. G., 2006, Asteroseismic inferences on GW Vir variable stars in the frame of new PG 1159 evolutionary models (arXiv:astro-ph/0603735)
[10] D'Antona F., Mazzitelli I., 1990a, araa, 28, 139
[11] D'Antona F., Mazzitelli I., 1990b, Annual Review of Astronomy and Astrophysics, 28, 139
[12] Deloye C., Bildsten L., 2002, Astrophysical Journal - ASTROPHYS J, 580, 1077
[13] Doherty C. L., Gil-Pons P., Siess L., Lattanzio J. C., Lau H. H. B., 2014, Monthly Notices of the Royal Astronomical Society, 446, 2599
[14] Dziembowski W. A., 1971, , 21, 289
[15] Eisenstein D. J., et al., 2006, The Astrophysical Journal Supplement Series, 167, 40
[16] Garcia-Berro E., Isern J., Hernanz M., 1997, mnras, 289, 973
[17] Gentile Fusillo N. P., et al., 2018, Monthly Notices of the Royal Astronomical Society, 482, 4570–4591
[18] Haft M., Raffelt G., Weiss A., 1994, The Astrophysical Journal, 425, 222
[19] Hansen B. M. S., Richer H., Kalirai J., Goldsbury R., Frewen S., Heyl J., 2015, The Astrophysical Journal, 809, 141
[20] Itoh N., Hayashi H., Nishikawa A., Kohyama Y., 1996, apjs, 102, 411
[21] Jiménez-Esteban F. M., Torres S., Rebassa-Mansergas A., Skorobogatov G., Solano E., Cantero C., Rodrigo C., 2018, Monthly Notices of the Royal Astronomical Society, 480, 4505
[22] Jr I., MacDonald J., 1985, The Astrophysical Journal, 296, 540
[23] Kantor E. M., Gusakov M. E., 2007, Monthly Notices of the Royal Astronomical Society, 381, 1702–1710
[24] Kawaler S. D., Bradley P. A., 1994, , 427, 415
[25] Kawaler S. D., Winget D. E., Hansen C. J., 1985, , 295, 547
[26] Kepler S. O., Kleinman S. J., Nitta A., Koester D., Castanheira B. G., Giovannini O., Costa A. F. M., Althaus L., 2007, Monthly Notices of the Royal Astronomical Society, 375, 1315
[27] Kepler S. O., et al., 2014, Monthly Notices of the Royal Astronomical Society, 446, 4078
[28] Kleinman S. J., et al., 2013, apjs, 204, 5
[29] Lamb D. Q., van Horn H. M., 1975, apj, 200, 306
[30] Lauffer G. R., Romero A. D., Kepler S. O., 2018, Monthly Notices of the Royal Astronomical Society, 480, 1547–1562
[31] Liebert J., Bergeron P., Holberg J. B., 2005, apjs, 156, 47
[32] Mestel L., 1952, Monthly Notices of the Royal Astronomical Society, 112, 583
[33] Munakata H., Kohyama Y., Itoh N., 1985, apj, 296, 197
[34] Nalezyty, M. Madej, J. 2004, A&A, 420, 507
[35] O'Brien M. S., Kawaler S. D., 2000, The Astrophysical Journal, 539, 372
[36] Paxton B., Bildsten L., Dotter A., Herwig F., Lesaffre P., Timmes F., 2010, The Astrophysical Journal Supplement Series, 192, 3
[37] Prusti T., et al., 2016, Astronomy & Astrophysics, 595
[38] Saio, H. 2013, EPJ Web of Conferences, 43, 05005
[39] Schwank D. C., 1976, , 43, 459
[40] Siess, L. 2006, A&A, 448, 717
[41] Tassoul M., 1980, The Astrophysical Journal Supplement Series, 43, 469
[42] Townsend R. H. D., Teitler S. A., 2013, Monthly Notices of the Royal Astronomical Society, 435, 3406
[43] Unno W., Osaki Y., Ando H., Shibahashi H., 1979, Nonradial oscillations of stars